GEOPHYSICAL RESEARCH LETTERS, VOL. 33, L16315, doi:10.1029/2006GL027079, 2006

Coseismic slip distribution of the 2003 M_w 6.6 San Simeon earthquake, California, determined from GPS measurements and seismic waveform data

F. Rolandone,[1] D. Dreger,[2] M. Murray,[2] and R. Bürgmann[2]

Received 5 June 2006; accepted 18 July 2006; published 30 August 2006.

[1] We combine geodetic and seismic data sets to constrain the coseismic slip distribution of the M_w6.6 San Simeon earthquake which occurred in the central California Coast Ranges on December 22, 2003. We use continuous and survey-mode GPS observations along with seismic waveform data from the California Integrated Seismic Network (CISN). We invert both data sets for the distribution of finite fault slip in a layered-Earth model. The inversion results indicate that the rupture extends to the southeast of the epicenter for approximately 25–30 km and occurred in a relatively shallow depth range between 1 to 10 km. The average and peak slip are 0.61 m and 2.37 m, respectively. The scalar seismic moment is 7.85e18 Nm, and the static stress drop 1.7 MPa. This thrust earthquake is characterized by its shallow, along-strike extended slip. **Citation:** Rolandone, F., D. Dreger, M. Murray, and R. Bürgmann (2006), Coseismic slip distribution of the 2003 M_w 6.6 San Simeon earthquake, California, determined from GPS measurements and seismic waveform data, *Geophys. Res. Lett.*, *33*, L16315, doi:10.1029/2006GL027079.

1. Introduction

[2] The M_w6.6 San Simeon earthquake struck the central California coast on December 22 2003, 50 km west of the San Andreas fault. The San Simeon earthquake is one of several destructive blind-thrust earthquakes. The main shock nucleated at a depth of 8–10 km and was followed by a vigorous aftershock sequence primarily southeast of the hypocenter, consistent with the main shock rupture propagation [*Hardebeck et al.*, 2004; *Hauksson et al.*, 2004]. The directivity of the rupture resulted in a concentration of damage to the southeast, with high levels of damage in Paso Robles.

[3] 35 GPS-measured surface offsets were combined with three-component seismic waveform data from 11 CISN sites to invert for the detailed kinematic rupture process. We present our preferred model and we discuss the implications of the model in terms of central Coast Range ground motion hazard.

2. GPS Data and Analysis

[4] We use data from 35 GPS sites in this study (Figure 1 and Tables S1 and S2 of the auxiliary material[1]). The San Simeon earthquake produced static displacements at 18 continuously operating GPS stations located within 70 km of the epicentral region. 13 stations are located northeast of the rupture near the Parkfield segment of the San Andreas fault.

[5] Many of the 17 survey-mode GPS sites are located within 40 km of the rupture. Following the San Simeon earthquake, we resurveyed 6 GPS stations northeast of the main shock. The USGS began continuously occupying 3 stations west of the epicenter one day after the event and another site southeast of the main shock one week later. Three sites east of the rupture were occupied by JPL within 3 days of the event. A survey of 4 additional sites south of the rupture was done 2 months after San Simeon by the USGS.

[6] We use the GAMIT/GLOBK GPS processing software to analyze the GPS data and combine our daily solutions and an appropriate set of global and regional solutions from the Scripps Orbital and Permanent Array Center (http://sopac.ucsd.edu). Preseismic and postseismic motions of campaign GPS sites can be significant and need to be quantified and removed to establish a valid estimate of coseismic offsets. Some of the sites have multiple years of measurements prior to the earthquake and have well established preseismic velocities. For some sites we use interseismic velocities from the SCEC Crustal Motion Map (http://epicenter.usc.edu/cmm3/). For sites not surveyed until 2 months after the earthquake we apply a postseismic model correction as described below.

[7] To estimate displacements due to the earthquake, we used two methods. For permanent sites we average the four days prior to and the four days following the earthquake. For the other sites, we estimate the position just before the earthquake using the older measurements and the interseismic velocity with the velocity uncertainty being propagated into the pre-earthquake position. We estimate the site offset based on the estimated pre-earthquake position and we only use the first four days of post-earthquake measurements to limit postseismic signal in the data. The four sites south of the rupture, surveyed 2 months after the earthquake, likely experienced significant postseismic displacements, and a postseismic correction was applied to them (Table S2). The observed postseismic deformation did not exceed about 22 mm and was mainly observed in the 10 days after the earthquake. This postseismic deformation may be mod-

[1] Laboratoire de Tectonique, UMR 7072, Université Pierre et Marie Curie, Paris, France.
[2] Berkeley Seismological Laboratory, University of California, Berkeley, California, USA.

0094-8276/06/2006GL027079$05.00

[1] Auxiliary material data sets available at ftp://ftp.agu.org/apend/gl/2006gl027079. Other auxiliary material files are in the HTML.

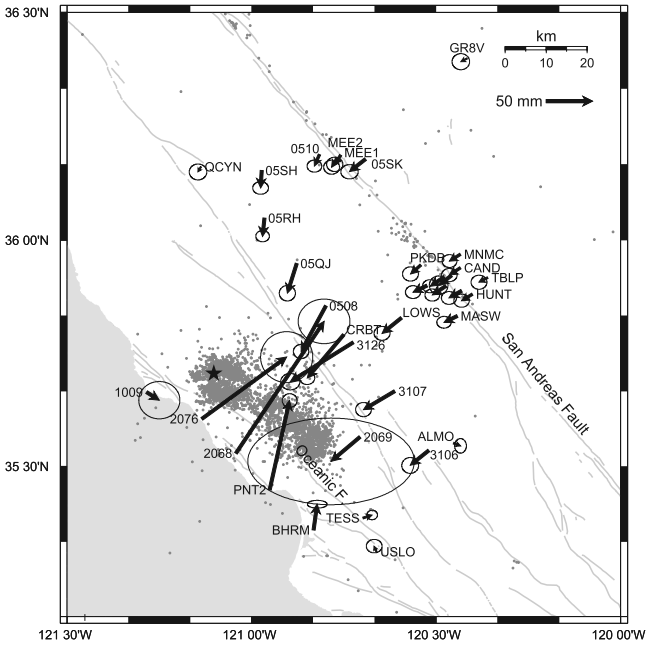

Figure 1. GPS sites and coseismic displacements from the M_w6.6 San Simeon earthquake with 95% confidence ellipses. The black star shows the epicenter, the dots show relocated aftershocks [*Hardebeck et al.*, 2004]. Surface fault traces are shown as grey lines.

elled as aseismic fault slip around the coseismic rupture at a depth of about 3 km.

3. Geodetic and Seismic Data Inversion for Fault Slip Model

[8] We use the geodetic data to constrain the rupture geometry. We model the observed coseismic displacements using rectangular dislocations in an elastic, homogeneous and isotropic half-space [*Okada*, 1985]. We use a constrained, nonlinear optimization algorithm [*Bürgmann et al.*, 1997], which allows us to estimate the geometry (parameterized by length, depth, width, dip, strike, and location) and the strike-slip and dip-slip offsets of one fault that best fit the GPS data. In addition, we performed over 42,000 linear inversions for slip distribution varying the strike, dip and rake (held constant over the fault surface). In the distributed slip inversions the model is parameterized with 2×2 km^2 subfaults over a 66 km by 22 km fault pinned at the hypocenter. Smoothing and slip positivity constraints [e.g., *Kaverina et al.*, 2002] are applied. The results of these inversions give an optimal fault model with a strike of 300°, a dip of 51° to the NE, and a rake of 76°. For the distributed slip case it is possible to fit the GPS data with a variance reduction of 95.9%. Results obtained using a layered elastic model are found to be the same (within 0.4% of modeling error). We find that both the optimal uniform-slip dislocation and the optimal distributed slip models are consistent with the seismological evidence. The San Simeon focal mechanism and the aftershock distribution suggest the Oceanic fault as the main rupture zone [*Hardebeck et al.*, 2004]. The Oceanic fault has a strike of about 292° near the epicenter and changes orientation to the south with a more northern strike similar to the one given by our geometry inversion. In the non-linear inversions our measure of misfit, the reduced χ^2 value, is not improved if we allow for a second dislocation in the geometry inversion.

[9] The geometry inversion results are used to constrain the fault model to invert for kinematic parameters and a slip distribution that best fits both the GPS and the seismic waveform data. The model is parameterized with 2 by 2 km elements distributed over 44 km along strike and 22 km down dip. We use a linear inversion for slip that allows for variable rake, rupture velocity and rise time [e.g., *Hartzell and Heaton*, 1983; *Dreger and Kaverina*, 2000; *Kaverina et al.*, 2002]. First a series of inversions assuming constant rupture velocity and rise time was performed. In this case rupture velocity ranging from 1 to 3.5 km/s and rise time from 0.5 to 5 seconds are tested using a grid search. The second series of inversions utilized multiple time windows to allow for spatially variable rupture velocity and rise time. In both cases the orientation of the fault and the rake are from the linear GPS inversion described above.

[10] In all of the inversions we combine displacement and velocity (for PKD) waveform data from 11 three-component CISN strong motion stations with 35 observations of GPS displacements to simultaneously invert for the distribution of fault slip. The weight between the geodetic and seismic waveform data is determined by trial and error to find a value that results in near-maximum levels of fit to both data sets. Additionally, there is an inverse distance weighting employed to equalize the variance of observations of nearby and distant seismic stations. As Figure 2 shows the seismic stations are reasonably well distributed around the source region.

[11] The waveform data are processed by deconvolving the instrument response, double integrating the recorded acceleration to displacement (PKD was integrated only to velocity), and high pass filtering above 0.01 Hz to remove long-period noise. A low-pass filter is not used. The seismic Green's functions are computed using frequency wave number integration and the GIL7 velocity model used to determine source parameters of events in the Coast Ranges. The GIL7 velocity model was developed from waveform modeling and is superior in modeling aftershock records at PKD compared to two P-wave arrival time models derived for the region. This analysis (Figures S6 and S7) shows that the GIL7 velocity model is the best choice for a source inversion. The GPS deformation Green's functions are computed for the same layered model using the method of *Wang et al.* [2006].

[12] The constant rupture velocity and rise time inversions have best fitting values of 2.6 km/s and 2 seconds, respectively. The rise time is relatively long for a M_w6.6 event, but consistent with the long-period nature of the unfiltered waveforms. The slip in these inversions is elongated along strike 30 km to the SE of the hypocenter and does not reach below 10 km depth. This model is able to fit the GPS and seismic waveform data with variance reductions of 94.6% and 43.7%, respectively.

[13] The second series of inversions were carried out using multiple time-windows to allow for variable rupture velocity and rise time. The rise time of each time window is 1 second, and the time windows are offset by 0.5 second. We use an omega-2 slip velocity function ($s(t) = t * \exp(-t/\tau)$,

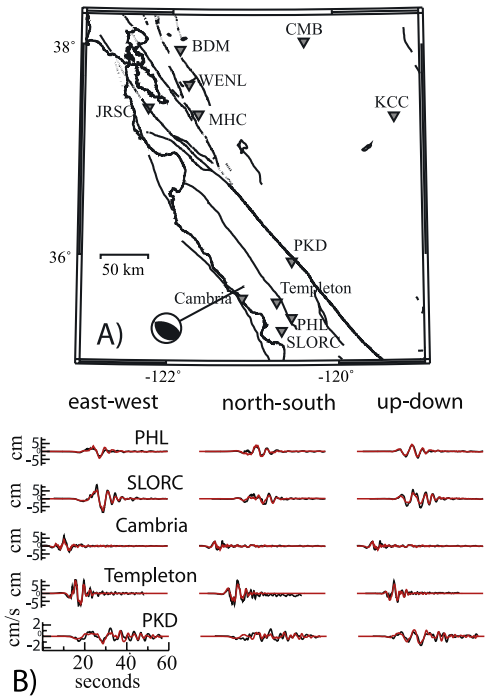

Figure 2. (a) Map showing the locations of seismic stations used in the slip inversions. The epicenter is indicated. (b) Comparison of observed (black) and simulated (red) displacement waveforms (velocity for PKD) for the preferred model allowing for variable rise time and rake angle and using both GPS and seismic waveform data. Quantitatively the fit to the seismic data is excellent with a 74% variance reduction.

where τ is a parameter controlling the width of the function). The results show that the rupture velocity is relatively constant, but that the rise time scales with the slip. On average the rise time is 2–3 seconds, though areas of the fault with smaller slip have shorter rise times. With this model it is possible to fit the GPS and seismic waveform data with variance reductions of 96.7% and 61.4%, respectively. The fit to the seismic waveform data is significantly improved.

[14] A final set of inversions were carried out in which the rake is allowed to vary over the fault in addition to the multiple time-windows as previously described. We also examine the sensitivity of the results to the assumed hypocenter depth. The hypocenter depth over the published range of 8–10 km has no significant effect on the kinematic modeling results (Figures S4 and S5), though slightly better fit is obtained for a depth of 8 km. The result of this inversion (Figure 3), for a hypocenter at 8 km, shows that the slip direction does not vary much over the fault, and that the slip is nearly pure reverse, significantly steeper than obtained previously inverting only the GPS data. In this case it is possible to fit the GPS and seismic waveform data with variance reductions of 95.6% and 74.0%, respectively. The fit to the seismic waveform data is again significantly improved, and the GPS fit remains high. Figure 2 shows the fit to the data for the preferred variable rake slip model shown in Figure 3. The average and peak slip are 0.61 m and 2.37 m, respectively. The scalar seismic moment in this model is 7.85e18 Nm corresponding to M_w6.6. The obtained scalar seismic moment is between the Berkeley Moment Tensor (6.0e18Nm) and the Harvard CMT (8.46e18 Nm) solutions.

[15] Slip in the model extends a total of 40 km SE, with the largest asperity located between 10–25 km away in a region with few aftershocks [e.g., *Hardebeck et al.*, 2004]. Generally, we find that all of the inversions produce similar results in terms of the depth of faulting and the extent of slip to SE, thus the GPS and seismic waveform data are consistent with each other. As additional time parameterization is employed to model rise time and rake variability we find that it is possible to significantly improve the fit to the seismic waveform data (43.7% to 74% variance reduction) without greatly changing the distribution of the slip and the fit to the GPS data. This indicates that the temporal complexity is important in modeling the seismic records of this earthquake. The obtained model is very similar to what *Ji et al.* [2004] obtained by inverting continuous 1 Hz GPS and local waveform data. The comparison is remarkably good considering that different data sets, finite-source parameterization, and inversion methods are used.

4. Discussion

[16] The event has a relatively long slip rise time function that is variable over the rupture surface with an average duration of about 2–3 seconds. Long rise times while unusual [e.g., *Heaton*, 1990] have been observed in other events (see, e.g., *Kaverina et al.* [2002] and *Ji et al.* [2002] for the 1999 Hector Mine earthquake). While the obtained rise time is longer than is typically seen (0.9 seconds for a M_w6.6 event [*Somerville et al.*, 1999]) it is about 0.2 to 0.3 times the total rupture time, and therefore the process is consistent with a self-healing slip pulse [*Heaton*, 1990]. The slip velocity varies from 0 to 0.64 m/s over the fault, and the average is 0.21 m/s. These values are consistent with what has been observed in other events.

[17] The along-strike extended nature of the slip is unusual. *Mai and Beroza* [2000] compiled 31 finite-source models for 18 strike-slip and reverse-slip earthquakes ranging in magnitude from M_w5.6 to 8.1, and obtained regression formulas for the scaling of fault length and width as well as other parameters. The aspect ratio (length/width) of faulting from their formulas for a M_w6.6 reverse slip event is 1.5. In contrast the aspect ratio of the 2003 San

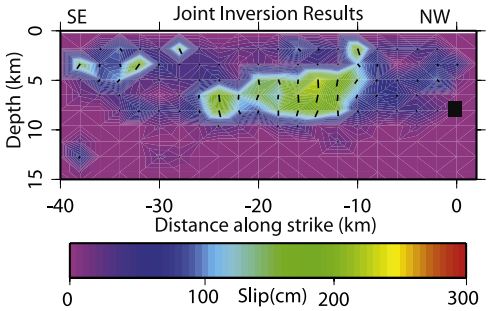

Figure 3. Shading shows the slip magnitude and the black bars show the slip direction. In this model the slip is nearly pure reverse. This model is able to fit the GPS and seismic waveform data to a very high degree as discussed in the text.

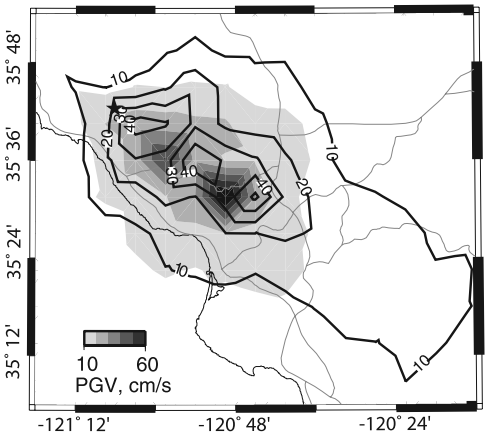

Figure 4. Simulated peak ground velocity assuming the obtained kinematic source description. Contours are in intervals of 10 cm/s. The surface projection of slip is shown. Simulated PGV for the actual reverse slip mechanism in shades of gray, and simulated PGV for a vertical right-lateral strike-slip mechanism plotted as contours.

Simeon earthquake is approximately 2.9 (25 divided by 9). In this sense the San Simeon earthquake is more similar to the 1999 Chi-Chi, Taiwan, M_w7.6 earthquake which had an aspect ratio of 2.8 (from the *Chi et al.* [2001] model).

[18] Dip-slip events with aspect ratios closer to 1 that nucleate deep tend to have pronounced updip directivity and elevated ground motions on the hanging block as was observed in the San Fernando and Northridge earthquakes. The 2003 San Simeon earthquake on the other hand has a lateral rupture process that elevated motions in the SE direction. However as shown by *Aagaard et al.* [2004] the directivity effect for laterally rupturing dip-slip faults is a minimum compared to other mechanisms.

[19] We use the obtained slip distribution to simulate near-fault peak ground velocity for the actual reverse-slip case and for a case of a vertically dipping right-lateral strike-slip fault (Figure 4). The plot clearly shows the southeastward extension of ground motion contours due to source finiteness and directivity. The two lobes of elevated ground velocity extending due east and due south of the earthquake are both 45 degrees from the strike direction and are the directivity-amplified SH lobes (maxima of SH radiation) of the reverse focal mechanism. In contrast, the strike-slip case shows a more pronounced SH maximum in the strike direction, and the area experiencing greater than 10 cm/s peak ground velocity is more than twice that of the dip-slip case. With models that had more continuous slip distributions, the difference is more pronounced where peak amplitudes can be 3 times higher and the 10 cm/s area 4 times greater in the strike-slip case (Figure S8). While directivity surely contributed to the high level of ground motions in Paso Robles it was less than could have occurred had the event been strike-slip. The last large nearby earthquake, the 1952 Bryson event, was predominantly strike-slip [*Dehlinger and Bolt*, 1987] and therefore consideration of strike-slip events should be considered in characterizing shaking hazard in the central Coast Ranges region. Finally, it is also important to note that had the San Simeon event been a more typical reverse event, ground motions in the updip direction and on the hanging block could have been more severe than experienced in 2003.

[20] **Acknowledgments.** We thank JPL, USGS, Caltrans, University of Wisconsin for providing GPS data. We acknowledge the helpful reviews of Fabrice Cotton and Gene Aaron Ichinose. This is BSL contribution 06-07.

References

Aagaard, B., J. Hall, and T. V. Heaton (2004), Effects of fault dip and slip rake angles on near-source ground motions: Why rupture directivity was minimal in the 1999 Chi-Chi, Taiwan, earthquake, *Bull. Seismol. Soc. Am.*, *94*, 155–170.

Bürgmann, R., P. Segall, M. Lisowski, and J. Svarc (1997), Postseismic strain following the 1989 Loma Prieta earthquake from GPS and leveling measurements, *J. Geophys. Res.*, *102*, 4933–4955.

Dehlinger, P., and B. Bolt (1987), Earthquakes and associated tectonics in a part of coastal central California, *Bull. Seismol. Soc. Am.*, *77*, 2056–2073.

Dreger, D., and A. Kaverina (2000), Seismic remote sensing for the earthquake source process and near-source strong shaking: A case study of the October 16, 1999 Hector Mine earthquake, *Geophys. Res. Lett.*, *27*, 1941–1944.

Chi, W. C., D. Dreger, and A. Kaverina (2001), Finite-source modeling of the 1999 Taiwan (Chi Chi) earthquake derived from a dense strong-motion network, *Bull. Seismol. Soc. Am.*, *91*, 1144–1157.

Hardebeck, J. L., et al. (2004), Preliminary report on the 22 December 2003, M 6.5 San Simeon, California earthquake, *Seismol. Res. Lett.*, *75*, 155–172.

Hartzell, S. H., and T. H. Heaton (1983), Inversion of strong ground motion and teleseismic waveform data for the fault rupture history of the 1979 Imperial Valley, California, earthquake, *Bull. Seismol. Soc. Am.*, *73*, 1553–1583.

Hauksson, E., D. Oppenheimer, and T. M. Brocher (2004), Imaging the source region of the 2003 San Simeon earthquake within the weak Franciscan subduction complex, central California, *Geophys. Res. Lett.*, *31*, L20607, doi:10.1029/2004GL021049.

Heaton, T. H. (1990), Evidence for and implications of self-healing pulses of slip in earthquake rupture, *Phys. Earth Planet Inter.*, *64*, 1–20.

Ji, C., D. J. Wald, and D. V. Helmberger (2002), Source description of the 1999 Hector Mine, California, earthquake, II. Complexity of slip history, *Bull. Seismol. Soc. Am.*, *92*, 1208–1226.

Ji, C., K. M. Larson, Y. Tan, K. W. Hudnut, and K. Choi (2004), Slip history of the 2003 San Simeon Earthquake constrained by combining 1-Hz GPS, strong motion, and teleseismic data, *Geophys. Res. Lett.*, *31*, L17608, doi:10.1029/2004GL020448.

Kaverina, A., D. Dreger, and E. Price (2002), The combined inversion of seismic and geodetic data for the source process of the 16 October 1999 *Mw*7.1 Hector Mine, California, earthquake, *Bull. Seismol. Soc. Am.*, *92*, 1266–1280.

Mai, P. M., and G. C. Beroza (2000), Source scaling properties from finite-source-rupture models, *Bull. Seismol. Soc. Am.*, *90*, 604–615.

Okada, Y. (1985), Surface deformation due to shear and tensile faults in a half-space, *Bull. Seismol. Soc. Am.*, *75*, 1135–1154.

Somerville, P. G., K. Irikura, R. Graves, S. Sawada, D. Wald, N. Abrahamson, Y. Iwasaki, T. Kagawa, N. Smith, and A. Kowada (1999), Characterizing crustal earthquake slip models for the prediction of strong ground motion, *Seismol. Res. Lett.*, *70*, 59–80.

Wang, R., F. Lorenzo Martin, and F. Roth (2006), PSGRN/PSCMP-a new code for calculating co- and post-seismic deformation, geoid and gravity changes based on the viscoelastic-gravitational dislocation theory, *Comp. Geosci.*, *32*, 527–541.

F. Rolandone, Laboratoire de Tectonique, UMR 7072, Université Pierre et Marie Curie, 4 place Jussieu, F-75252 Paris, France. (frederique.rolandone@lgs.jussiue.fr)

D. Dreger, M. Murray, and R. Bürgmann, Berkeley Seismological Laboratory, University of California, Berkeley, CA 94720, USA.